


Article

New Insights into Sea Turtle Propulsion and Their Cost of Transport Point to a Potential New Generation of High-Efficient Underwater Drones for Ocean Exploration

Nick van der Geest * , Lorenzo Garcia * , Roy Nates and Fraser Borrett

BioDesign Lab, Auckland University of Technology, Auckland 1010, New Zealand

* Correspondence: nicky.van.der.geest@aut.ac.nz (N.v.d.G.); lorenzo.garcia@aut.ac.nz (L.G.)

Abstract: Sea turtles gracefully navigate their marine environments by flapping their pectoral flippers in an elegant routine to produce the required hydrodynamic forces required for locomotion. The propulsion of sea turtles has been shown to occur for approximately 30% of the limb beat, with the remaining 70% employing a drag-reducing glide. However, it is unknown how the sea turtle manipulates the flow during the propulsive stage. Answering this research question is a complicated process, especially when conducting laboratory tests on endangered animals, and the animal may not even swim with its regular routine while in a captive state. In this work, we take advantage of our robotic sea turtle, internally known as Cornelia, to offer the first insights into the flow features during the sea turtle's propulsion cycle consisting of the downstroke and the sweep stroke. Comparing the flow features to the animal's swim speed, flipper angle of attack, power consumption, thrust and lift production, we hypothesise how each of the flow features influences the animal's propulsive efforts and cost of transport (COT). Our findings show that the sea turtle can produce extremely low COT values that point to the effectiveness of the sea turtle propulsive technique. Based on our findings, we extract valuable data that can potentially lead to turtle-inspired elements for high-efficiency underwater drones for long-term underwater missions.

Keywords: sea turtles; underwater robots; underwater flight; soft robotics; biomimicry; animal biomechanics; CFD; fluid dynamics



Citation: van der Geest, N.; Garcia, L.; Nates, R.; Borrett, F. New Insights into Sea Turtle Propulsion and Their Cost of Transport Point to a Potential New Generation of High-Efficient Underwater Drones for Ocean Exploration. *J. Mar. Sci. Eng.* **2023**, *11*, 1944. <https://doi.org/10.3390/jmse11101944>

Academic Editor: Diego Villa

Received: 27 August 2023

Revised: 18 September 2023

Accepted: 29 September 2023

Published: 9 October 2023



Copyright: © 2023 by the authors. Licensee MDPI, Basel, Switzerland. This article is an open access article distributed under the terms and conditions of the Creative Commons Attribution (CC BY) license (<https://creativecommons.org/licenses/by/4.0/>).

1. Introduction

Sea turtles navigate their marine environments by gracefully flapping their pectoral wings/flippers to produce a visually enchanting locomotive pattern. This flapping motion allows the sea turtle migration of thousands of kilometres to reach favourable breeding or feeding grounds [1–5]. The flapping motion has typically been described as asymmetric, with the downstroke approximately twice as fast as the upstroke [6–8]. In recent work by van der Geest et al. [6], the flapping motion was described three-dimensionally for the Green sea turtle (*Chelonia mydas*), including the soft twisting of the flipper. The authors described the flipper motion by breaking it up into five segments consisting of the Downstroke (DS), Sweep stroke (SS), Recovery stroke one (RS1), Upstroke (US) and, finally, Recovery stroke two (RS2) (Figure 1). It is understood that during the Green turtle's general flapping routine, the upstroke does not generate any thrust [6,8–10]; however, during this time, the animal's drag coefficient is lowered to help reduce swim speed losses [10]. To quantify how the drag is reduced during the upstroke, van der Geest et al. [10] conducted dedicated work to uncover the flow features generated by the flipper during this period. Through dye visualisation of a scale turtle model in a towing tank, they found the flipper enters a near-equilibrium state that produces near-constant pressure across the entire flipper surface [10] (Movie S1). The constant pressure across the surface of the flipper then cancels out any flow mixing due to pressure differences, including the wing tip vortex. However, though this work is insightful, it does not cover what flow features occur during the sea turtles

(*Chelonia mydas*) propulsive cycle consisting of the downstroke and sweep stroke. The propulsion cycle in sea turtles has been previously described as only occurring during the downstroke period, with peak thrust occurring at the end of the downstroke [8,9], with the most recent works taking very different approaches to uncover the propulsive cycle. David T. Booth [9] found the propulsive cycle by studying green turtle hatchlings in a flume, while van der Geest et al. [8] developed a full-scale robotic sea turtle based on the green turtle that could reproduce the natural animals swimming patterns. Though both these works offered comparable insights into thrust production and/or energy consumption, they did not detail the flow features and fluid mechanical mechanisms responsible for the propulsion. David T. Booth [9] hypothesised the downstroke likely produces both lift-based and drag-based propulsion depending on the flipper angle of attack; however, what does lift-based or drag-based propulsion in sea turtles look like? And is this hypothesis accurate? To the best of our knowledge, no research details the flow features and fluid mechanical interactions sea turtles utilise during their downstroke using genuine sea turtle kinematics. However, work has been produced that analysed simplified two-dimensional turtle-inspired flow features [11,12]. Though these two-dimensional examples may offer insight, they fail to reproduce three-dimensional effects such as spanwise flow and Coriolis effects that have been shown as essential factors in biological flapping wings [13].

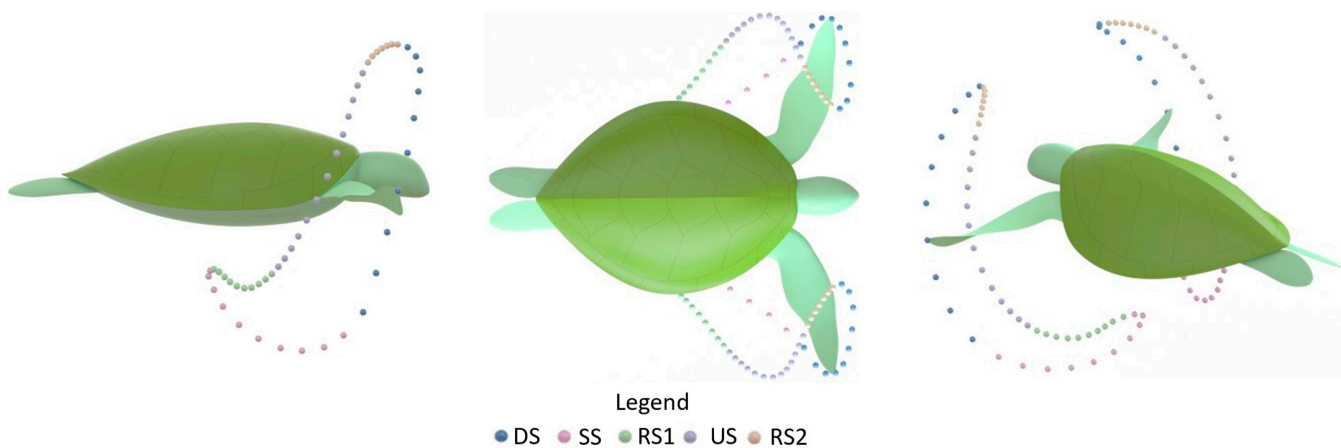


Figure 1. The wild sea turtle (*Chelonia mydas*) flipper pattern during the animal's regular swimming routine obtained from van der Geest et al. [6].

For the last 20 years, it has been well understood that the flow feature responsible for high-performance force production in biological flapping wings is the leading-edge vortex (LEV) [14–16]. The LEV has been shown to occur across all categories of animal species [14,15,17,18], with insect flight first believed to be a paradox before its discovery [14]. However, although the LEV has been heavily studied in flapping wings, to the best of our knowledge, no research exists for LEV generation during the downstroke in sea turtles that applies genuine and accurate sea turtle kinematics.

Recent studies into the propulsion methods of sea lions demonstrated that the sea lion's flippers create additional thrust by applying a clapping motion [19,20]. The clapping motion entrains fluid momentum on the low-pressure side of the flipper (dorsal side) that later develops into complex vortex shedding to increase thrust [19]. It is now understood that sea turtles also create a clapping motion referred to as the sweep stroke (Figure 1). However, the fluid interaction during the sea turtle's sweep stroke is entirely unknown.

Obtaining the flow features of sea turtles requires solving two significant complications. First, it is necessary to obtain animal ethical approval to conduct the test on endangered species; second, the animal may not even swim with its regular swim pattern while in a captive state [6,8,10]. To overcome such hurdles, we take advantage of our robotic sea turtle (Cornelia). Cornelia is the world's first and only robotic sea turtle that accurately produces the sea turtle's natural form and function, as detailed in our previous work [8]. This makes

Cornelia an invaluable tool for studying the fluid-structure interactions of turtles without the need to trouble the actual animal.

In this work, with the help of Cornelia, we break down each of the observed flow features of the turtle's flippers during the propulsive cycle (Figure 2). To the best of our knowledge, this is the first study to show insight into the flow features of the sea turtle during the animal's propulsive cycle. We compare the observed flow features against the turtle's thrust and lift forces flipper angle of attack (AoA), flipper velocity and power consumption, to offer insight into the ways in which each feature influences the animal's propulsion effort and cost of transport (COT). We compare the COT obtained by Cornelia against the current state-of-the-art swimming robotics [21–29], and we find Cornelia to produce extremely low values for the COT, pointing to the effectiveness of the sea turtle propulsive strategy.

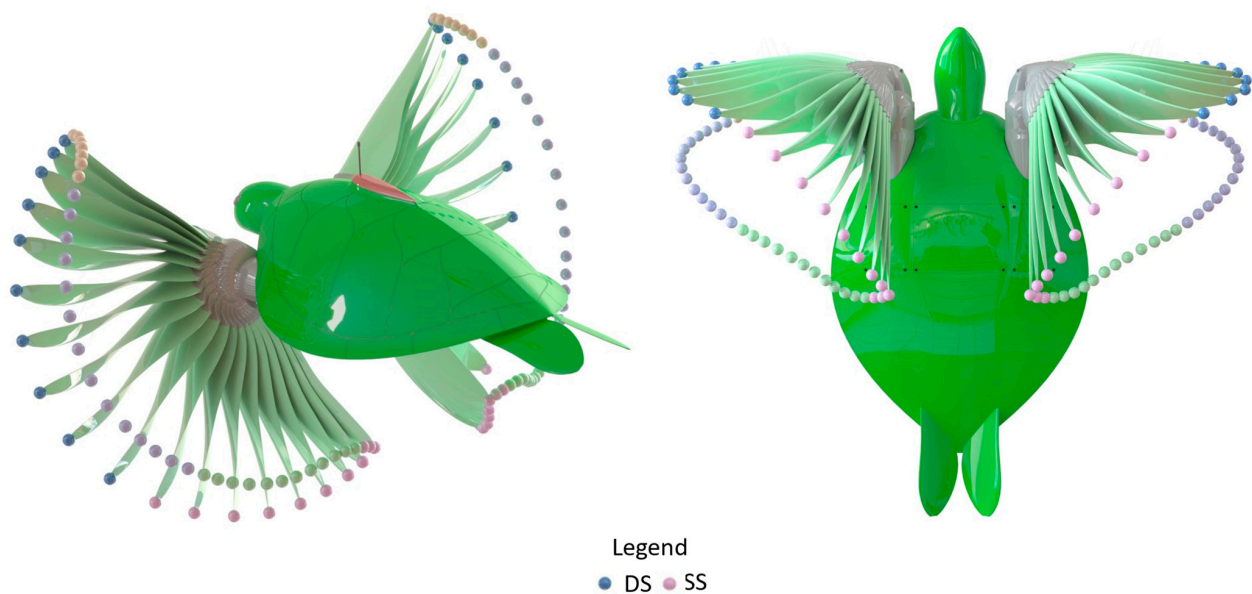


Figure 2. The robotic sea turtle (*Cornelia*) illustrating the propulsive cycle consisting of the downstroke and sweep stroke [8]. Also, see Movie S2.

Based on our findings, we hypothesise what practical aspects of the turtle's locomotion pattern could be developed and optimised to enhance the next generation of underwater drones and robotic technologies.

2. Methods

2.1. Method Overview

All tests were performed using our ad hoc testing rig, internally known as the “turtle dyno”, as shown in Figure 3. Testing involved towing the robot quickly up to speed before the robot taking over to propel itself. The turtle dyno recorded lift, drag, thrust, swim velocity and power consumption simultaneously during each test. The design and specification for the turtle dyno, along with a detailed analysis of the force production during the regular swimming routine, can be found in our previous work [8], so we do not cover this in detail here.

Due to its cost effectiveness and ease of application, individual flow features were observed using dye visualisation with our in-house developed dye application tools. CFD was additionally used to help complement the field tests and provide a deeper comprehension of the flow field characteristics.

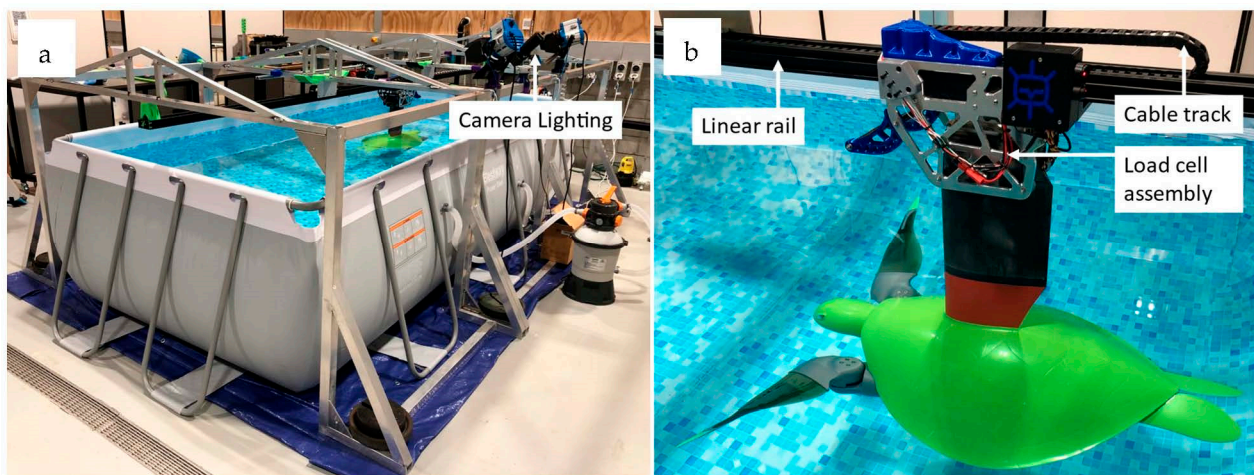


Figure 3. Turtle dynamometer. (a) Complete dynamometer assembly showing camera lighting arrangement. (b) Close-up of robot attached to load cell and linear rail assembly.

2.2. CFD Calculations

In parallel with laboratory experiments, commercial CFD tools were used to help better comprehend the flow features observed during physical testing with ANSYS Fluent (ANSYS 2021 R2, Canonsburg, PA, USA). Simulations only involved studying the flow around the rear flippers and during the sea turtle downstroke. The sweep stroke was not simulated due to its complex motion coupled with the complex wing morphing during this part of the locomotion pattern, thus creating high computational expense that was not available for this study. Additionally, it must be noted that the CFD simulations from this study were conducted not to produce highly accurate results, but to help complement the results from our laboratory experiments.

Two separate simulations were set up with the $k\omega$ SST model used to study the ways in which the flow from the turtle's carapace travels downstream to meet the rear flippers, and the realisable $k\epsilon$ model was used for simulating the downstroke due to its lower computational expense. The $k\omega$ model had the mesh refined down to a y^+ of 0.75, with the $k\epsilon$ model using a y^+ of 13.15 with the addition of scalable wall functions. As the turtle's downstroke applies a relatively constant wing twist [10] and a simple rotation motion, the simulation was simplified into two separate domains: a rotating domain with the flipper using a rigid body and a sliding mesh interface paired with a static domain (Figure S1a). The rotational domain angular velocity and velocity inlet values were established based on the values achieved by sea turtles during the downstroke period. The computational domain that used with the $k\omega$ model can be seen in Figure S1b, with a body of influence for mesh refinement added around the turtle body and further downstream to capture the wake produced by the turtle body. A symmetry boundary condition was used to substantially lower computational expense with a constant velocity inlet defined based on the turtle's average swimming velocity.

2.3. Dye Visualisation

To visualise the individual flow features during the regular swimming routines, we operated our in-house developed dye visualisation tools (Figure 4). The tools have been successfully used in our previous studies [10]; however, the streamline tool, as seen in Figure 4a, was further developed for this study, introducing up to 3 dye streamlines. The central pylon section of the tool used a NACA 0010 cross-section with each of the three stacked bodies using a 360° revolution of the NACA 0010 cross-section. The tool ran on a linear rail parallel to the turtle swim path and could have the dye accurately injected when required. To ensure the tool did not generate a significant disturbance in its wake, tests were performed to inject a cloud of dye into its path and record the disturbance in the wake (Figure 4c and Movie S3). Our testing suggested that the tool created insignificant

disturbance compared to the disturbance an animal in the wild would likely encounter, so we deemed the tool satisfactory for use. Flow features were recorded using high-speed underwater photography (Chronos 2.1HD 32GB, Kron Technologies Inc, Burnaby, BC, Canada) at full HD 1000 FPS and an action camera (GoPro Hero 10, GoPro, San Mateo, CA, USA) at full HD 240 FPS. The Chronos cameras were installed into waterproof housings (Salty surf housings, North Wollongong, NSW, Australia) and equipped with a Sigma 18–35 mm lens (Sigma Corporation, Kawasaki, Kanagawa, Japan).

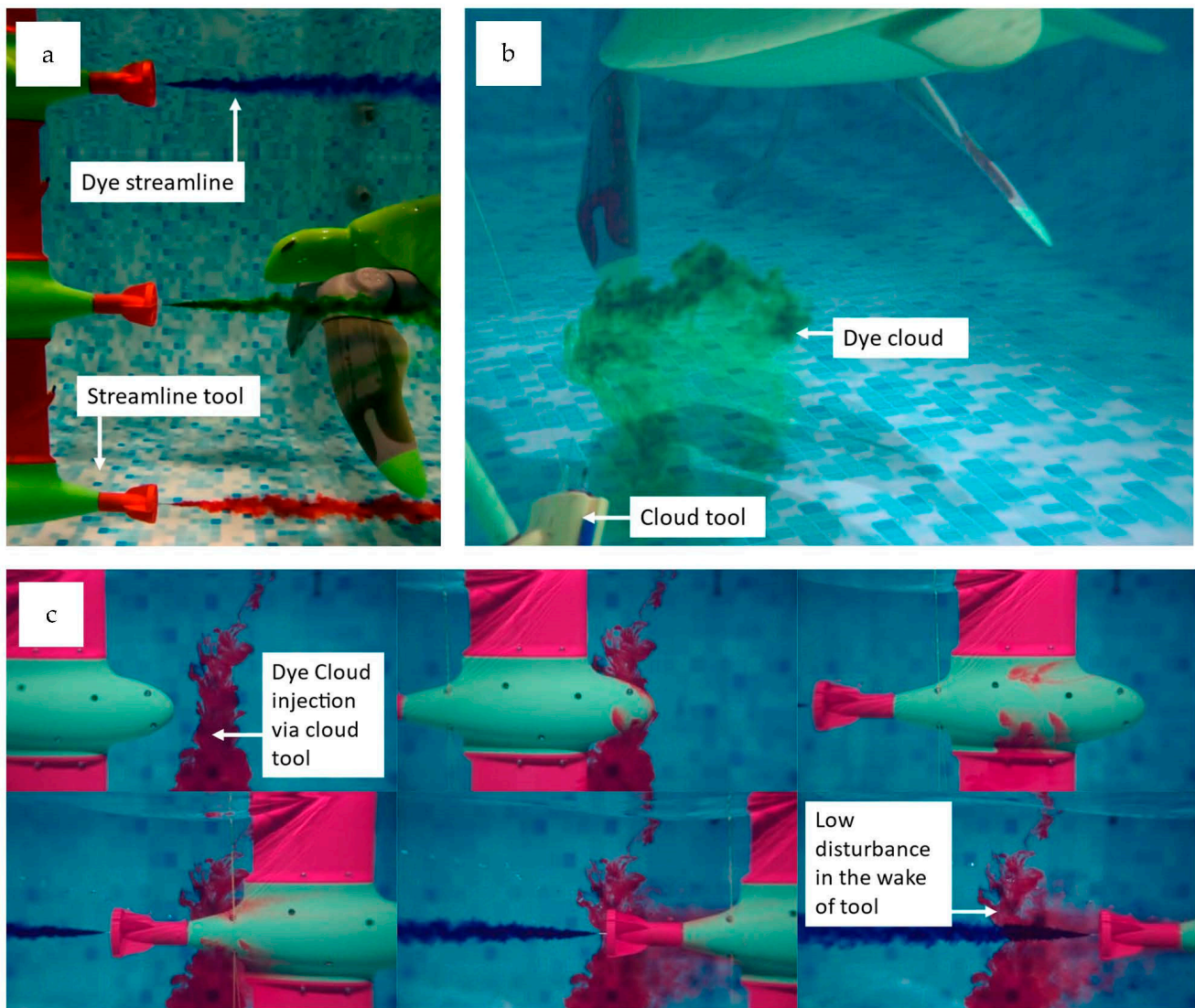


Figure 4. Dye visualisation tools. (a) Streamline tool in use. (b) Cloud tool in use. (c) Streamline tool wake disturbance testing. Also, see Movie S3.

3. Results and Discussion

3.1. Results Overview

As observed in Figure 5, all test results for thrust, lift, AoA, power, swim speed, and flipper tip velocity are detailed for the sea turtles DS and SS, with the corresponding flow features observed at each time interval detailed in Figure 5g. All tests were performed with the flapping frequency remaining constant at 0.23 Hz based on the average flapping observed in wild green sea turtles [6,8,30].

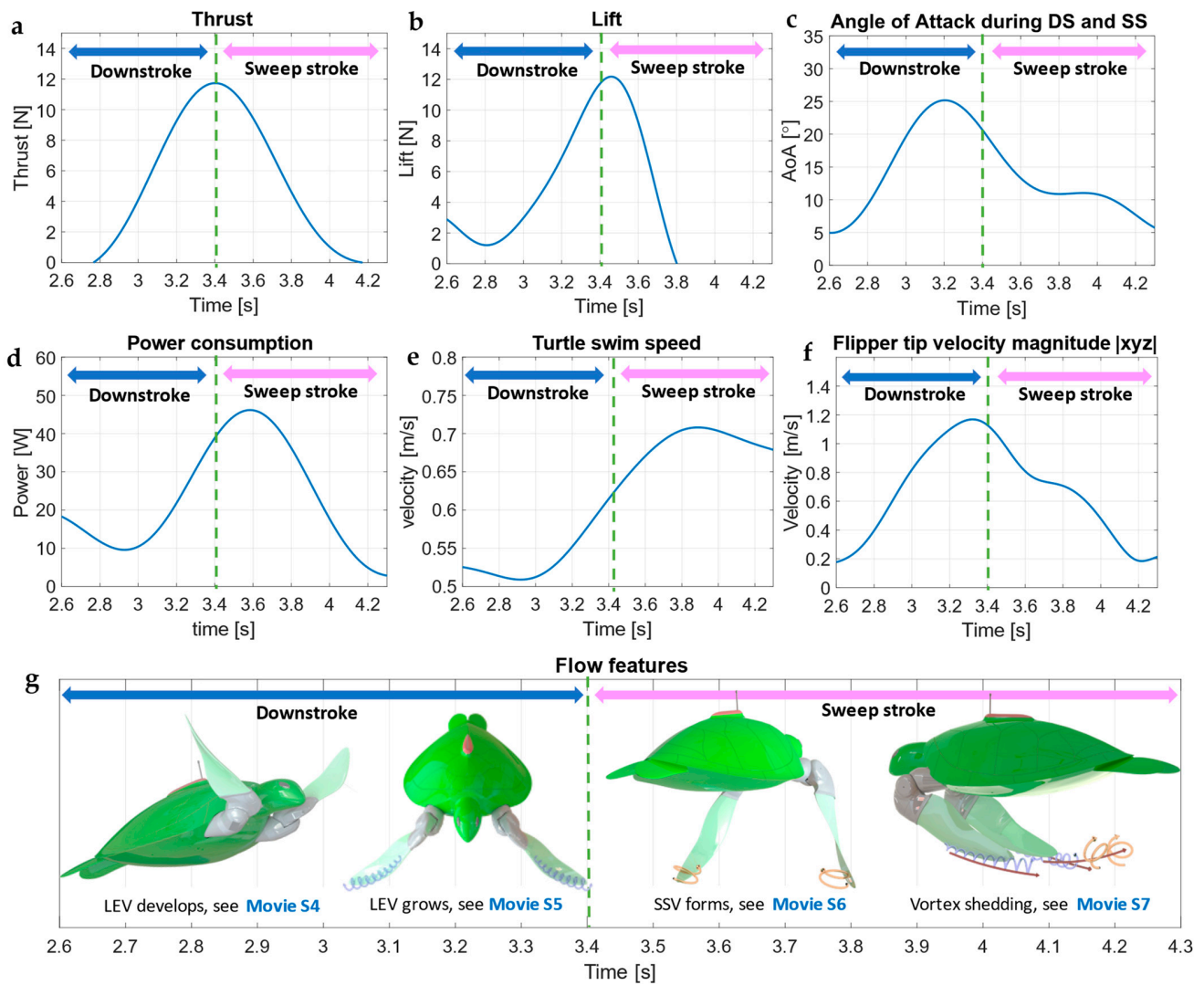


Figure 5. Plots of swimming performance of Cornelia for the Green sea turtle’s regular swimming routine. (a) Thrust production during the downstroke and the sweep stroke obtained from van der Geest et al. [8]. (b) Lift production during the downstroke and the sweep stroke obtained from van der Geest et al. [8]. (c) The average Angle of Attack across wingspan. See Figure S3 for exact AOA values across the flipper span. (d) Power consumption during the downstroke and the sweep stroke obtained from van der Geest et al. [8]. (e) Turtle swim speed during the downstroke and the sweep stroke obtained from van der Geest et al. [8]. (f) The flipper tip velocity magnitude during the downstroke and the sweep stroke. (g) For the timing of the observed flow features, see Movies S4–S7.

Testing was conducted by applying the sea turtle’s regular swimming routine at a Reynolds number of 367,000, defined as

$$Re = \frac{uD_{SCL}}{\nu}$$

Re was based on the average swim velocity (u) and straight carapace length (D_{SCL}). As the Reynolds number is established simply on steady, time-independent conditions [31], the Periodic Swimming Number (P) was also considered in this study, defined as

$$P = \frac{10u}{\sqrt{4\pi f\nu}}$$

where f is the flapping frequency and ν is the kinematics viscosity. The Periodic Swimming Number (P) was first introduced by Gurka et al. [31] as an adaptation of the Reynolds number to eliminate the need to choose a characteristic length scale and incorporate the animal’s periodic motion. Applying this, we found that the sea turtle swims at a value of 3537. This puts sea turtles approximately in the same range of P as Macaroni and Adelie penguins (3729–3882), along with Harp and Ringed seals (3330–3569) [31]. Additionally, the Strouhal number (St) was calculated to be 0.24 and defined as

$$St = \frac{D_{pp}f}{u},$$

where D_{pp} is the sea turtle’s flipper tip peak-to-peak distance during its regular swimming routine. This value of the Strouhal number puts sea turtles into a range of 0.2 to 0.4, as found in other swimming and flying animals tuned for high power efficiency [32–34].

3.2. Flipper Angle of Attack (AoA)

To help understand the flow feature contribution based on the relative flow around the turtle flippers during the downstroke and the sweep stroke, the AoA of the turtle’s flipper was defined as

$$\theta_{AoA} = \theta_p \pm \theta_f,$$

where θ_p is the spanwise twisting of the turtle’s flipper given as a linear piecewise function with respect to time as

$$\theta_p = \begin{cases} a_{p1}t, & 0 \leq t < t_1 \\ a_{p2}, & t_1 \leq t < t_2 \\ a_{p3}t + b_{p3}, & t_2 \leq t < t_3 \\ a_{p4}t + b_{p4}, & t_3 \leq t < t_4 \\ a_{p5}, & t_4 \leq t < t_5 \\ a_{p6}t + b_{p6}, & t_5 \leq t < t_6 \end{cases}$$

where a_{pn} and b_{pn} are the function constants. The relative flow direction θ_f on the turtle’s flipper was added or subtracted depending on the stage of motion that the flipper was in (upstroke or downstroke). This was done to provide a positive AoA for the relative flow acting on the ventral side of the flipper and a negative AoA when acting at the dorsal side (Figure S2). θ_f was calculated with

$$\theta_f = \arctan \left(\frac{\sqrt{\dot{y} + \dot{z}}}{V_s + \dot{x}} \right),$$

where V_s represents the swimming speed of the turtle, while \dot{x} , \dot{y} and \dot{z} signify the velocity components at any given point on the turtle’s flipper. These velocity components are obtained by taking the time derivative of the flipper position function, which was formulated using a Fourier series with

$$\dot{x} = V_f \left(\sum_{i=1}^n -i\omega_x a_{ix} \sin(i\omega_x t) + i\omega_x b_{ix} \cos(i\omega_x t) \right),$$

$$\dot{y} = V_f \left(\sum_{i=1}^n -i\omega_y a_{iy} \sin(i\omega_y t) + i\omega_y b_{iy} \cos(i\omega_y t) \right),$$

$$\dot{z} = V_f \left(\sum_{i=1}^n -i\omega_z a_{iz} \sin(i\omega_z t) + i\omega_z b_{iz} \cos(i\omega_z t) \right),$$

where n is set to eight terms, a_i and b_i are the Fourier coefficients and w is the fundamental frequency. The velocity modifier (V_f) to correct the velocity for any point along the span of the turtle's flipper was represented with $V_f = \frac{x_s}{s}$, x_s representing any point along the flipper span (s). As the twisting of the flipper is a linear relationship [10], the exact amount of wing twist at any point along the flipper span (s) was calculated with $\theta(x) = \frac{\theta_p x_s}{s}$. Shown in Figure 5c, the average AoA is plotted by calculating each value at various points along the flipper span.

3.3. Downstroke

During the initial stages of the DS, there was no reliable evidence of any substantial vortex formation on the turtle's flippers with relatively smooth flow conditions during this phase in time. This is predominately due to the low AoA during the early DS and low flipper tip velocity, resulting in low thrust, lift and power consumption. At an approximately 2.8 s mark, clear evidence of a LEV forming along the turtle's wing can be seen along with substantial spanwise flow from the wing root to the wing tip (Figure 6 and Movie S4). As the downstroke progresses, the wing tip velocity increases to reach a maximum at the end of the downstroke, where the LEV is at its most forceful stage, with thrust and lift reaching their maximum values (Movie S5). This finding differs from past research hypotheses that depict the large force production at the end of the sea turtle downstroke as being drag-based due to high AoA [9]. Additionally, in Figure 5c,f, the wing AoA begins to bleed off before the flipper reaches its maximum velocity and force production, revealing that high force production is more accurately associated with higher wing velocities and more aggressive LEV formation. Additionally, as the LEV delays wing stall [15,18,35] by forcing the flow to reattach to the low-pressure/dorsal side (Figure 6a–d and Movie S4), this suggests the entire downstroke is completely lift-based propulsion during the sea turtle's regular swimming routine.

3.4. Sweep Stroke

The sweep stroke begins at approximately 3.4 to 3.5 s into the turtle flapping routine, with the LEV remaining attached during the sweep strokes duration. During the entire sweep stroke, the AoA, flipper velocity, power consumption, thrust and lift begin to lower, with the turtle reaching a maximum swim speed approximately 50% into the sweep stroke stage. At a roughly 3.6 to 3.7 s mark, a vortex forms that is almost immediately shed into the turtle's wake (Figure 5g and Movie S6). We name this vortex the sweep stroke vortex (SSV), and in contrast to the LEV, the SSV rotates in the opposite direction and is produced by the wing's ventral side (high-pressure side).

Near the end of the sweep stroke, the flippers are brought parallel beneath the carapace to create a clapping motion similar to the sea lion [19,20]. At this point, the LEV is shed from the wing's dorsal side into the wake to follow behind the SSV (Figure 5g and Movie S7). Just before the LEV is shed into the wake, it entrains fluid momentum on the dorsal side of the flipper (Movie S7), similar to the sea lion [19]. In sea lions, this helps contribute to downstream momentum when the vortex structure is shed to add additional thrust [19]. Based on our observed flow features, this downstream momentum can also be assumed to happen with sea turtles, additionally, as the thrust curve towards the end of the stroke bleeds off rather than simply dropping off like the lift forces (Figure 5a,b). At this point, the sea turtle enters a glide that lasts for 70% of the overall limb beat cycle [8,10]. During the glide, the sea turtle shapes its flippers to generate a passive upstroke to recover its flippers into a position ready for the downstroke to help with energy expenditure [8,10].

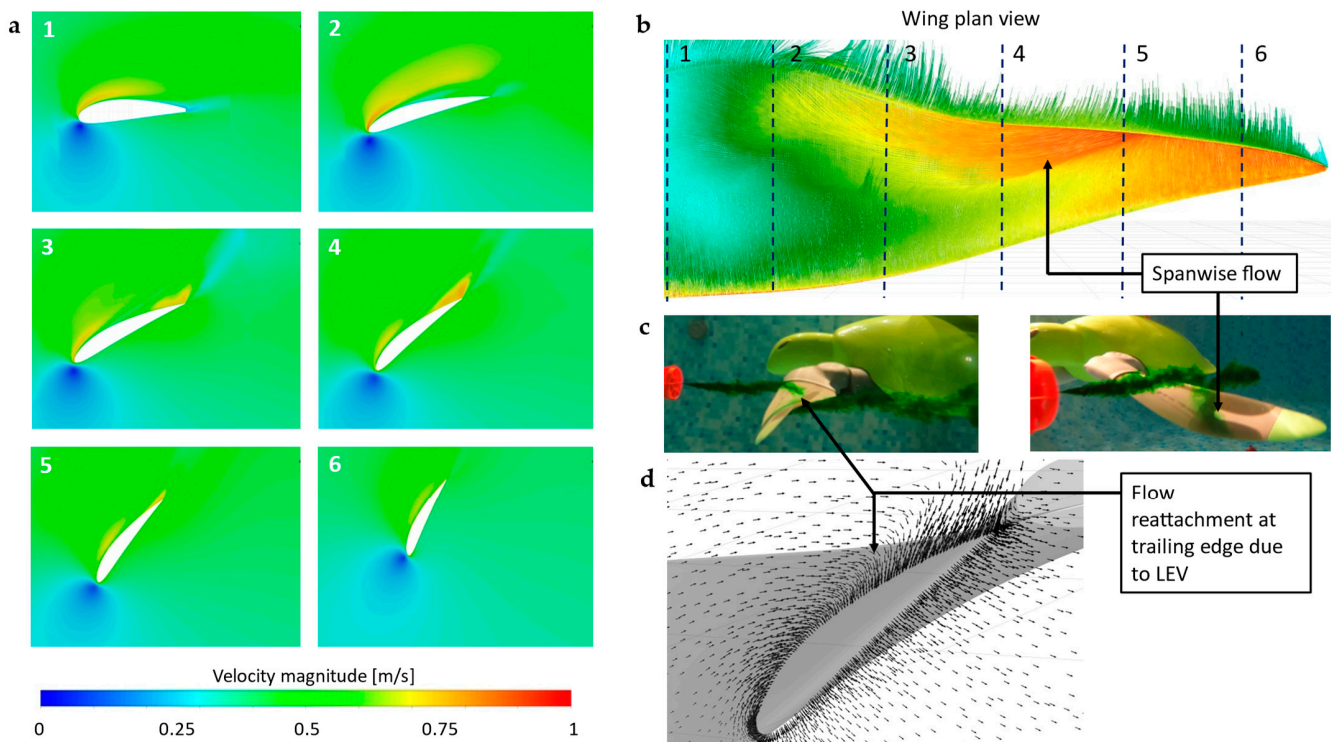


Figure 6. Downstroke flow features. (a) Velocity plots from various cross-sections along the turtle’s wingspan from CFD. The numbers 1–6 in the top left of each cross-section correlate to the dashed lines shown in Figure 6b. (b) Plan view of the turtle wing showing cross-section locations and velocity streamlines obtained from CFD. (c) Dye visualisation testing shows flow reattachment towards the wing trailing edge and the spanwise flow demonstrated by dye being transported towards the wing tip. (d) Vector plot from CFD showing flow reattachment.

3.5. Rear Flippers

During the turtle’s regular swimming routine, van der Geest et al. [6] documented that the rear flippers are seen to tuck in behind the carapace with the flipper tips pointing backwards and near motionless as per Figure 7. Our CFD and field test results show that towards the rear of the carapace, the flow detaches from shell to create a low energy zone directly where the rear flippers are positioned (Figure 7c,d and Movie S8). This volume of low energy flow helps lower the form and friction drag on the turtle’s rear flippers, thus improving the animal’s drag coefficient for the gliding stage. This also helps explain why the flippers remain almost motionless, as any changes to the flipper’s position within this low energy zone may not generate any significant directional control for the turtle.

3.6. Turtle Swimming Efficiency and Cost of Transport

As observed in Figure 8, the power consumption, thrust production and swim speed data are plotted from the experimental swimming tests for the complete swimming cycle. Additionally, a curve of input power (Figure 8a) divided by output thrust (Figure 8b) is displayed for the down- and the sweep strokes in Figure 8e with the cost of transport (COT) for the complete swimming cycle detailed in Table 1 and plotted against time in Figure 8d. The cost of transport was calculated with

$$COT = \frac{P_{in}}{mgu'}$$

where P_{in} is the input power (Figure 8a), m is the mass of Cornelia, g is the acceleration due to gravity and u is the swimming velocity (Figure 8c). During the regular swimming routine, Cornelia produced an average COT for the entire swimming cycle of only 0.072

to generate one of the lowest *COT* values in literature for a swimming robot (Table 1). This is largely due to the propulsion strategy, where the sea turtle produces propulsion for approximately 30% of the limb beat cycle, with the remaining 70% producing a power-saving glide that does not reduce swimming velocity substantially due to the animal’s large mass and low drag coefficient [8]. This points to the effectiveness of this swimming strategy and helps explain the ability of sea turtles to swim such vast distances with minimal energy intake.

Cornelia demonstrated that the most energy-efficient point during the propulsion stage was at the 3.1 s mark, generating a power-to-thrust ratio of approximately 2 W/N or 7 N of thrust for 14 W electrical input power (Figure 8e). At this point, the AoA was almost at its maximum value, and the sea turtle had already begun accelerating its velocity from its power-saving glide. Additionally, the LEV continued to grow, with the lift forces producing approximately 5 N of upward force.

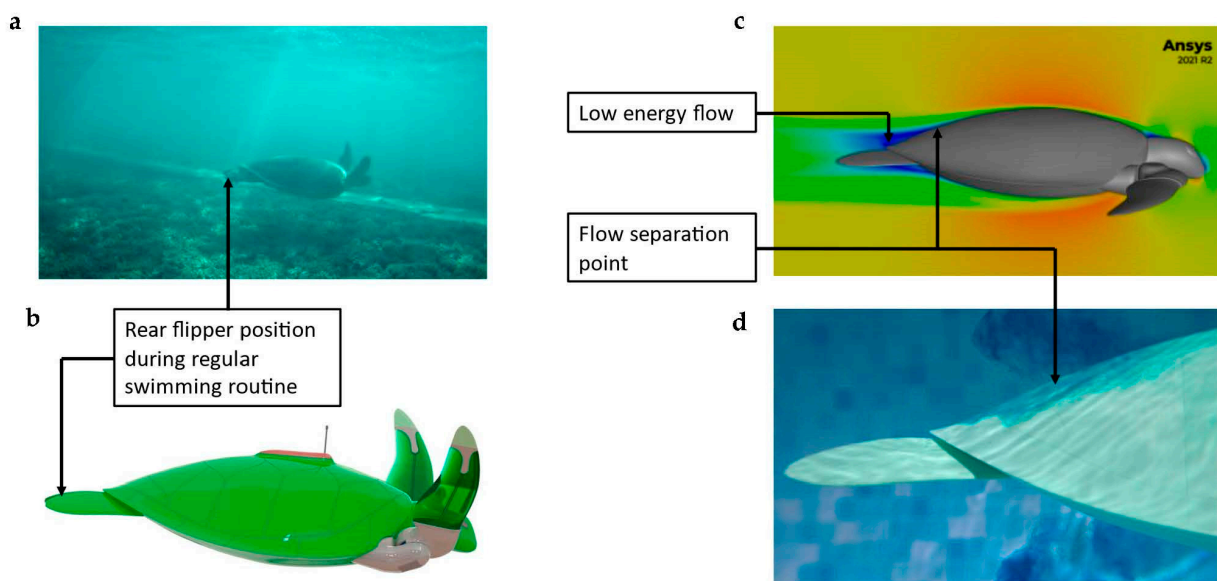


Figure 7. Flow over the sea turtle’s rear flippers during its regular swimming routine. (a) A wild sea turtle producing the 5-stage locomotion cycle, demonstrating the rear flipper position. (b) Cornelia replicates the wild sea turtle in (a). (c) CFD results showing a velocity contour of the flow around the rear the flippers. (d) Dye visualisation tests showing flow separation point. Also see Movie S8.

Table 1. Cost of transport of recent state-of-the-art swimming robots from the literature.

COT in Recent State-of-the-Art Swimming Robot	COT	Data Obtained From
Cornelia	0.072	Results from this current study
ART	3	Baines et al. [24]
Eel inspired robot	10.72	Nguyen et al. [21]
Flexible swimming robot	2.5	Kwak et al. [22]
FINBOT	8.2	Berlinger et al. [23]
Squid-inspired robot	0.087	Bujard et al. [25]
Flexible robotic fish	0.293	Lu et al. [26]
Tunabot	2.83	Zhu et al. [27]
Tunabot flex	1.876	White et al. [28]
HASEL jellyfish	1.619	Wang et al. [29]

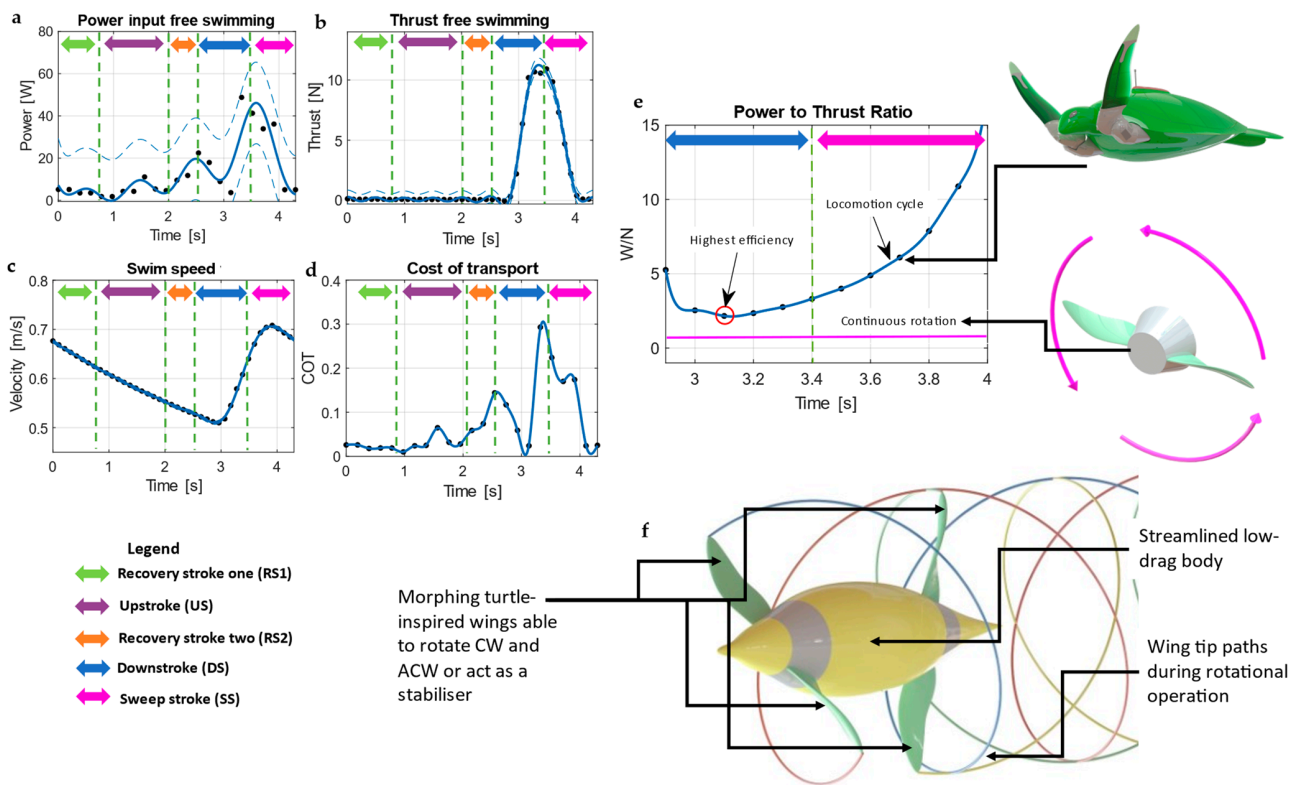


Figure 8. Turtle swimming efficiency. (a) Power input data for the complete swimming cycle obtained from van der Geest et al. [8]. (b) Thrust production for the complete swimming cycle obtained from van der Geest et al. [8]. (c) Turtle swim speed for complete swim cycle obtained from van der Geest et al. [8]. (d) Cost of transport plotted against time. (e) The power-to-thrust ratio plotted for the downstroke and the sweep stroke compared to the power-to-thrust ratio of a continuous rotating turtle wing. (f) Turtle-inspired propulsion applied to a low-drag streamlined body. Diagram illustrating a tandem configuration with both sets of wings/flippers generating propulsion (also see Movie S9).

Overall, we found the downstroke was more efficient than the sweep stroke; however, this could be due to the sweep stroke requiring all six servo motors to run simultaneously, contrary to the downstroke, which only required two servo motors to run heavily. Additionally, the motors used in Cornelia’s robotic limbs are hobby-grade servo motors that we believe may have low mechanical efficiency.

Though the *COT* obtained is impressive, employing a flapping winged machine in a commercial drone or device for ocean exploration is far from practical, and the multi-degree of freedom wings produce complex maintenance procedures coupled with highly complex manufacturing. For the findings produced here to be valuable, practicable and obtainable for industry-level technology, we combined the essential variables consisting of wing twist, wingtip velocity and wing shape to generate a CFD simulation of a continuously rotating turtle wing to continuously harness the most efficient section of the turtle locomotive cycle, as previously mentioned at the 3.1 s mark. Our results demonstrated that it was possible to achieve a maximum sustained power-to-thrust ratio of 0.5 W/N or 8 N of thrust for 4 W mechanical input power (Figure 8e).

When comparing the thrust values of the continuously rotating turtle wing against the sea turtle locomotive cycle, it can be observed that the thrust values are comparable with the CFD results producing 8 N and Cornelia producing 7 N during the standard sea turtle locomotive cycle. However, there are variations when comparing the power values, as the CFD results do not include the overall electrical efficiency of the servo motors and electronics. Therefore, the significant difference in power consumption likely originates from two main factors: first, the efficiency of the electro-mechanical system, and second,

as the turtle's flipper is accelerating at this point, it creates additional power consumption when compared to the constant velocity rotating model.

The continuously rotating turtle wing model could offer significant potential for enhancing propulsion technologies, especially in multi-functional applications. Beyond the clear energy-saving merits, incorporating a morphing rotating propulsor reveals an array of advantages for aquatic navigation and energy harvesting. Illustrated in Figure 8f and further elucidated in Movie S9, applying a set of morphing sea turtle-inspired propulsors in a tandem orientation attached to a low-drag streamlined fuselage could facilitate a multi-purpose underwater drone. While one set of wings concentrates on propulsion, the other functions as a stabiliser. This configuration promotes consistent and controlled motion, bolstering the vessel's stability—a crucial attribute for peak performance across diverse aquatic conditions.

Furthermore, as the wings morph, they can transition into a counter-rotating setup. Such an arrangement is paramount for neutralising the rotational forces exerted on the vessel's fuselage due to the torque from a singular propeller set. This ensures that the vessel's trajectory remains unaffected by undesired rotations. Additionally, the concept of torque vectoring can be explored; by dynamically adjusting the Angle Of Attack (AOA) of each wing or flipper at precise moments, the vessel may achieve unparalleled underwater agility.

Taking cues from the biomechanics of sea turtles, the device has the potential to function as a sea glider. In certain conditions, energy can be harnessed by back-spinning the propellers. This mechanism is reminiscent of how sea turtles leverage their upstroke to optimise energy use. Thus, this could evolve beyond its foundational propulsion capabilities to also serve as a renewable energy harvester, seamlessly integrating navigation proficiency with sustainable energy solutions.

4. Conclusions and Future Work

In conclusion, this study examines the sea turtle's propulsive cycle considering the downstroke and the sweep stroke during the animal's regular swimming routine. The findings reveal a critical characteristic that may account for their highly efficient swimming performance, including their capacity to generate considerable thrust and lift forces during the downstroke phase, with a continuous LEV formation during both downstroke and sweep stroke, until it is shed into the wake at the end of the sweep stroke to hypothetically contribute towards downstream momentum similarly to sea lions [19].

Additionally, the study highlights that the Green sea turtle robot, *Cornelia*, produces one of the lowest Cost of Transport (COT) values in the literature for a swimming robot, indicating the effectiveness of the sea turtle swimming strategy for long-distance swimming with minimal energy intake. This underscores the potential for the incorporation of these principles into the design and operation of marine robots and other aquatic devices. Their low COT values are likely due to their efficient energy usage through a combination of active propulsion and passive gliding stages. This, coupled with the rear flippers' tucking motion into a zone of low energy flow, can reduce the form and friction drag the turtle experiences, thus improving its drag coefficient for the gliding stage.

Despite the energy-efficient flapping cycle exhibited by sea turtles, applying these findings to commercial drones or ocean exploration devices remains a challenge due to the complexity of their locomotion. Yet, by capturing the most efficient section of the turtle's locomotion cycle and simulating a continuously rotating turtle wing, our study offers promising avenues for developing industry-level technology.

Though this work brings new insight into the flow features during the sea turtle's propulsive cycle, it is difficult to pinpoint the exact effect of each flow feature and how these features interact with each other to generate the animal's propulsion. A deeper understanding of this can be achieved in future work with the utilisation of a high-level PIV system. Additionally, as these findings are for regular straight-line swimming, our

robot Cornelia can be programmed to study the ways in which the animal creates its manoeuvring techniques by building in the required control systems.

In summary, this research provides novel insights into the flow features and COT of sea turtle locomotion and offers valuable guidance for the future development of efficient aquatic propulsion systems.

Supplementary Materials: The following supporting information can be downloaded at: <https://www.mdpi.com/article/10.3390/jmse11101944/s1>, Supplementary Figures S1 to S3; Supplementary Movies S1 to S9.

Author Contributions: Conceptualisation: N.v.d.G., L.G., R.N. and F.B.; Methodology: N.v.d.G., L.G. and R.N.; Investigation: N.v.d.G., L.G., R.N. and F.B.; Visualisation: N.v.d.G., L.G. and R.N.; Funding acquisition: L.G.; Project administration: L.G. and R.N.; Supervision: L.G. and R.N.; Writing—original draft: N.v.d.G., L.G., R.N. and F.B.; Writing—review and editing: N.v.d.G., L.G., R.N. and F.B. All authors have read and agreed to the published version of the manuscript.

Funding: This work was partially funded by the Science for Technological Innovation project, AUTX2101 Bio-inspired Underwater Robot for Ocean Surveillance and Protection PROP-80135-NSCSEED-AUT, Ministry of Business, Innovation and Employment, New Zealand.

Institutional Review Board Statement: Not applicable.

Informed Consent Statement: Not applicable.

Data Availability Statement: All data sets for the current study are available from the authors on reasonable request via contacting the corresponding authors.

Acknowledgments: To Nick's family, friends and lab colleagues (Gary van der Geest, Bronwyn van der Geest, Lena Straub, Keegan van der Geest, Corry van der Geest, Trystan van der Geest, Anton van der Geest, Hannah Pyles, Mike Noakes, Adam Murly, Bastian Busch, Mike Norris, Harsimran Singh and Ricky Liang) for spending their weekends with the research team to conduct data collection and testing. To MAG Assembly LTD and Grant Burrell for their expert craftsmanship in painting our robotic sea turtle with a newly formulated colour named "Pearlescent Turtle Green".

Conflicts of Interest: The authors declare no conflict of interest.

References

- Hays, G.C.; Scott, R. Global patterns for upper ceilings on migration distance in sea turtles and comparisons with fish, birds and mammals. *Funct. Ecol.* **2013**, *27*, 748–756. [[CrossRef](#)]
- Eckert, S.A. High-use oceanic areas for Atlantic leatherback sea turtles (*Dermochelys coriacea*) as identified using satellite telemetered location and dive information. *Mar. Biol.* **2006**, *149*, 1257–1267. [[CrossRef](#)]
- Heaslip, S.G.; Iverson, S.J.; Bowen, W.D.; James, M.C. Jellyfish Support High Energy Intake of Leatherback Sea Turtles (*Dermochelys coriacea*): Video Evidence from Animal-Borne Cameras. *PLoS ONE* **2012**, *7*, e33259. [[CrossRef](#)]
- Alerstam, T.; Hedenström, A.; Åkesson, S. Long-distance migration: Evolution and determinants. *Oikos* **2003**, *103*, 247–260. [[CrossRef](#)]
- Luschi, P.; Hays, G.C.; Del Seppia, C.; Marsh, R.; Papi, F. The navigational feats of green sea turtles migrating from Ascension Island investigated by satellite telemetry. *Proc. R. Soc. Lond. Ser. B Biol. Sci.* **1998**, *265*, 2279–2284. [[CrossRef](#)]
- van der Geest, N.; Garcia, L.; Nates, R.; Godoy, D.A. New insight into the swimming kinematics of wild Green sea turtles (*Chelonia mydas*). *Sci. Rep.* **2022**, *12*, 18151. [[CrossRef](#)]
- Davenport, J.; Munks, S.A.; Oxford, P.J. A Comparison of the swimming of Marine and Freshwater Turtles. *R. Soc. London. Ser. B Biol. Sci.* **1984**, *220*, 447–475. [[CrossRef](#)]
- van der Geest, N.; Garcia, L.; Borret, F.; Nates, R.; Gonzalez, A. Soft-robotic green sea turtle (*Chelonia mydas*) developed to replace animal experimentation provides new insight into their propulsive strategies. *Sci. Rep.* **2023**, *13*, 11983. [[CrossRef](#)]
- Booth, D.T. Kinematics of swimming and thrust production during powerstroking bouts of the swim frenzy in green turtle hatchlings. *Biol. Open* **2014**, *3*, 887–894. [[CrossRef](#)]
- van der Geest, N.; Garcia, L.; Nates, R.; Gonzalez-Vazquez, A. Sea Turtles Employ Drag-Reducing Techniques to Conserve Energy. *J. Mar. Sci. Eng.* **2022**, *10*, 1770. [[CrossRef](#)]
- Izraelevitz, J.S.; Triantafyllou, M.S. Adding in-line motion and model-based optimisation offers exceptional force control authority in flapping foils. *J. Fluid Mech.* **2014**, *742*, 5–34. [[CrossRef](#)]
- Licht, S.C.; Wibawa, M.S.; Hover, F.S.; Triantafyllou, M.S. In-line motion causes high thrust and efficiency in flapping foils that use power downstroke. *J. Exp. Biol.* **2010**, *213*, 63–71. [[CrossRef](#)] [[PubMed](#)]
- Jardin, T. Coriolis effect and the attachment of the leading edge vortex. *J. Fluid Mech.* **2017**, *820*, 312–340. [[CrossRef](#)]

14. Johansson, L.C.; Engel, S.; Kelber, A.; Heerenbrink, M.K.; Hedenstrom, A. Multiple leading edge vortices of unexpected strength in freely flying hawkmoth. *Sci. Rep.* **2013**, *3*, 3264. [[CrossRef](#)]
15. Nabawy, M.R.A.; Crowther, W.J. The role of the leading edge vortex in lift augmentation of steadily revolving wings: A change in perspective. *J. R. Soc. Interface* **2017**, *14*, 20170159. [[CrossRef](#)]
16. Birch, J.M.; Dickinson, M.H. Spanwise flow and the attachment of the leading-edge vortex on insect wings. *Nature* **2001**, *412*, 729–733. [[CrossRef](#)]
17. Menzer, A.; Gong, Y.; Fish, F.E.; Dong, H. Bio-Inspired Propulsion: Towards Understanding the Role of Pectoral Fin Kinematics in Manta-like Swimming. *Biomimetics* **2022**, *7*, 45. [[CrossRef](#)]
18. Videler, J.J.; Stamhuis, E.J.; Povel, G.D.E. Leading-Edge Vortex Lifts Swifts. *Science* **2004**, *306*, 1960–1962. [[CrossRef](#)]
19. Kashi, E.; Kulkarni, A.A.; Perrotta, G.; Leftwich, M.C. Flowfields produced by a robotic sea lion foreflipper starting from rest. *Bioinspir. Biomim.* **2020**, *15*, 035002. [[CrossRef](#)]
20. Liu, Y.; Li, H.; Deng, S.; Wang, S.; Liu, S.; Wang, Z. Biomimetic Robotic Sea Lion Foreflippers: Design, Modeling, and Experimentation. *IEEE ASME Trans. Mechatron.* **2022**, *27*, 5679–5689. [[CrossRef](#)]
21. Nguyen, D.Q.; Ho, V.A. Anguilliform Swimming Performance of an Eel-Inspired Soft Robot. *Soft Robot.* **2022**, *9*, 425–439. [[CrossRef](#)] [[PubMed](#)]
22. Kwak, B.; Choi, S.; Bae, J. Development of a Stiffness-Adjustable Articulated Paddle and its Application to a Swimming Robot. *Adv. Intell. Syst.* **2023**, *5*, 2200348. [[CrossRef](#)]
23. Berlinger, F.; Saadat, M.; Haj-Hariri, H.; Lauder, G.V.; Nagpal, R. Fish-like three-dimensional swimming with an autonomous, multi-fin, and biomimetic robot. *Bioinspir. Biomim.* **2021**, *16*, 026018. [[CrossRef](#)] [[PubMed](#)]
24. Baines, R.; Patiballa, S.K.; Booth, J.; Ramirez, L.; Sipple, T.; Garcia, A.; Fish, F.; Kramer-Bottiglio, R. Multi-environment robotic transitions through adaptive morphogenesis. *Nature* **2022**, *610*, 283–289. [[CrossRef](#)] [[PubMed](#)]
25. Bujard, T.; Giorgio-Serchi, F.; Weymouth, G.D. A resonant squid-inspired robot unlocks biological propulsive efficiency. *Sci. Robot.* **2021**, *6*, eabd2971. [[CrossRef](#)]
26. Lu, B.; Zhou, C.; Wang, J.; Zhang, Z.; Tan, M. Toward Swimming Speed Optimization of a Multi-Flexible Robotic Fish With Low Cost of Transport. *IEEE Trans. Autom. Sci. Eng.* **2023**, *20*, 1–12. [[CrossRef](#)]
27. Zhu, J.; White, C.; Wainwright, D.K.; Di Santo, V.; Lauder, G.V.; Bart-Smith, H. Tuna robotics: A high-frequency experimental platform exploring the performance space of swimming fishes. *Sci. Robot.* **2019**, *4*, eaax4615. [[CrossRef](#)]
28. White, C.H.; Lauder, G.V.; Bart-Smith, H. Tunabot Flex: A tuna-inspired robot with body flexibility improves high-performance swimming. *Bioinspir. Biomim.* **2021**, *16*, 026019. [[CrossRef](#)]
29. Wang, T.; Joo, H.J.; Song, S.; Hu, W.; Keplinger, C.; Sitti, M. A versatile jellyfish-like robotic platform for effective underwater propulsion and manipulation. *Sci. Adv.* **2023**, *9*, eadg0292. [[CrossRef](#)]
30. Yasuda, T.; Arai, N. Changes in flipper beat frequency, body angle and swimming speed of female green turtles *Chelonia mydas*. *Mar. Ecol. Prog. Ser.* **2009**, *386*, 275–286. [[CrossRef](#)]
31. Gurka, R.; Nafi, A.S.; Weihs, D. On an adaptation of the Reynolds number, applicable to body-caudal-fin aquatic locomotion. *Front. Mar. Sci.* **2022**, *9*, 914214. [[CrossRef](#)]
32. Taylor, G.K.; Nudds, R.L.; Thomas, A.L.R. Flying and swimming animals cruise at a Strouhal number tuned for high power efficiency. *Nature* **2003**, *425*, 707–711. [[CrossRef](#)] [[PubMed](#)]
33. Eloy, C. Optimal Strouhal number for swimming animals. *J. Fluids Struct.* **2012**, *30*, 205–218. [[CrossRef](#)]
34. Triantafyllou, G.S.; Triantafyllou, M.S.; Grosenbaugh, M.A. Optimal Thrust Development in Oscillating Foils with Application to Fish Propulsion. *J. Fluids Struct.* **1993**, *7*, 205–224. [[CrossRef](#)]
35. Carr, L.W.; Chandrasekhara, M.S. Compressibility effects on dynamic stall. *Prog. Aerosp. Sci.* **1996**, *32*, 523–573. [[CrossRef](#)]

Disclaimer/Publisher’s Note: The statements, opinions and data contained in all publications are solely those of the individual author(s) and contributor(s) and not of MDPI and/or the editor(s). MDPI and/or the editor(s) disclaim responsibility for any injury to people or property resulting from any ideas, methods, instructions or products referred to in the content.